Çukurova Üniversitesi Mühendislik Fakültesi Dergisi, 38(3), ss. 725-738, Eylül 2023
Cukurova University Journal of the Faculty of Engineering, 38(3), pp. 725-738, September 2023

Comparison of a Dynamic Model of Electric Arc Furnace with Actual Operation Data for Voltage Flicker Analysis in Electrical Power Network

Tahsin KÖROĞLU[*1] **ORCID** *0000-0002-6587-3529*

[1]*Adana Alparslan Turkes Science and Technology University, Faculty of Engineering, Department of Electrical & Electronics Engineering, Adana, Türkiye*

Geliş tarihi: 21.08.2023 Kabul tarihi: 29.09.2023

Atıf şekli/ How to cite: KÖROĞLU, T., (2023). Comparison of a Dynamic Model of Electric Arc Furnace with Actual Operation Data for Voltage Flicker Analysis in Electrical Power Network. Cukurova University, Journal of the Faculty of Engineering, 38(3), 725-738.

Abstract

Electric arc furnaces (EAFs) used in the iron and steel manufacturing industry for melting and refining scrap metals are one of the most disturbing loads that exhibit unbalanced and highly nonlinear characteristics. Serious voltage fluctuations occur in the power system as a result of the rapid change in the current drawn from the grid by the EAF. Voltage fluctuations lead to a power quality problem known as flicker, which is defined as observable changes in light sources that affect the production environment, cause eye fatigue in personnel, and lower the work concentration levels. To investigate the voltage flicker problem, an accurate mathematical model describing the behavior of the EAF load is required. In this study, a dynamic EAF model that can be adjusted to different operating conditions has been developed in the time domain. The electric arc voltage has been modeled as an externally controllable voltage source. The instantaneous arc voltage has been expressed as a function of the arc length independent of the current. The arc resistance, which varies with time and is nonlinear, has also been calculated with differential equations using the instantaneous arc voltage value. To measure the short-term flicker severity index caused by the EAF in the power system, a flicker meter in compliance with the International Electrotechnical Commission (IEC) 61000-4-15 standard has been designed. The current-voltage characteristics of the EAF, its effect on the power system, and the flicker severity occurring at the point of common coupling (PCC) have been analyzed with simulation studies using the PSCAD/EMTDC software. Besides, the simulation results of the dynamic model of the EAF have been compared with the results obtained from the model based on the measured field data.

Keywords: Electric arc furnace, Flicker, Power quality, Flickermeter

Elektrik Güç Şebekesi'nde Gerilim Titreşim Analizi için Elektrik Ark Ocağının Dinamik Modeli ile Gerçek Çalışma Verilerinin Karşılaştırılması

Öz

Demir-çelik imalat sanayinde hurda metallerin ergitilmesi ve rafine edilmesi için kullanılan elektrik ark ocakları (EAF'leri), dengesiz ve oldukça doğrusal olmayan özellikler sergileyen en rahatsız edici yüklerden

[*]Sorumlu yazar (Corresponding Author): Tahsin KÖROĞLU, *tkoroglu@atu.edu.tr*

biridir. EAF'nin şebekeden çektiği akımın hızla değişmesi sonucu güç sisteminde ciddi gerilim dalgalanmaları meydana gelir. Gerilim dalgalanmaları, ışık kaynaklarında üretim ortamını etkileyen gözlemlenebilir değişiklikler olarak tanımlanan, personelde göz yorgunluğuna ve iş konsantrasyon düzeylerinin düşmesine neden olan ve kırpışma olarak bilinen bir güç kalitesi sorununa yol açar. Gerilim kırpışma problemini araştırmak için, EAF yükünün davranışını açıklayan doğru bir matematiksel modele ihtiyaç vardır. Bu çalışmada, zaman domeninde farklı çalışma koşullarına göre ayarlanabilen dinamik bir EAF modeli geliştirilmiştir. Elektrik ark gerilimi, harici olarak kontrol edilebilen bir gerilim kaynağı olarak modellenmiştir. Anlık ark gerilimi, akımdan bağımsız olarak ark uzunluğunun bir fonksiyonu olarak ifade edilmiştir. Zamanla değişen ve doğrusal olmayan ark direnci de anlık ark gerilimi değeri kullanılarak diferansiyel denklemlerle hesaplanmıştır. Güç sisteminde EAF'nin neden olduğu kısa süreli kırpışma şiddeti indeksini ölçmek için Uluslararası Elektroteknik Komisyonu (IEC) 61000-4-15 standardına uygun bir kırpışma ölçer tasarlanmıştır. EAF'nin akım-gerilim karakteristiği, güç sistemine etkisi ve ortak bağlantı noktasında (PCC) oluşan kırpışma şiddeti, PSCAD/EMTDC yazılımı kullanılarak simülasyon çalışmaları ile analiz edilmiştir. Ayrıca, EAF'nin dinamik modelinin simülasyon sonuçları, ölçülen saha verilerine dayalı modelden elde edilen sonuçlarla karşılaştırılmıştır.

Anahtar Kelimeler: Elektrik ark ocağı, Kırpışma, Güç kalitesi, Kırpışma ölçer

1. INTRODUCTION

In recent years, the number of electric arc furnace (EAF) installations has increased significantly due to the abundance of scrap metal in the iron and steel industry, the need for recycling waste metals, and the possibility of high metal production at a relatively low cost [1]. However, such loads have adverse effects on power quality because of their extremely nonlinear and time-variable (dynamic) features [2]. The EAF operation causes flicker, harmonics, interharmonics, current/voltage imbalances, and severely changing reactive power demand [3, 4]. Flicker is due to the fluctuation of the voltage that exceeds a certain amplitude versus frequency curve representing the eye–brain–lamp sensitivity, and has a negative impact on people [5].

Figure 1 shows a typical power system of an EAF consisting of a utility grid, source impedance (Z_s), high-voltage/medium-voltage (HV/MV) power transformer, serial reactor, EAF transformer, and EAF with three electrodes [6].

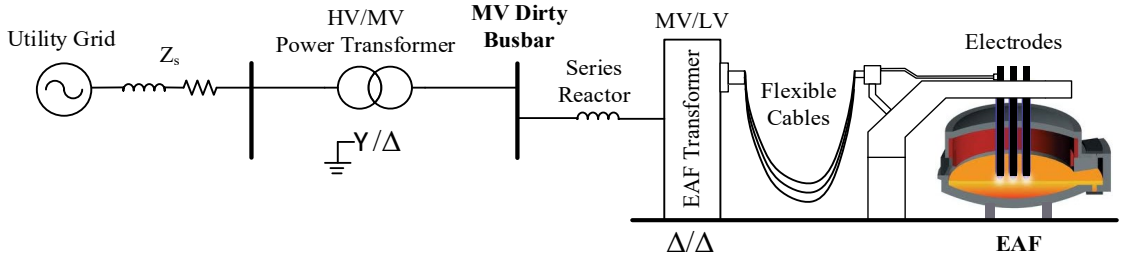

Figure 1. Power system of the EAF

EAF is an extremely hot enclosed space, where heat is produced by means of an electrical arc for melting scrap steel without changing its electrochemical properties [7]. In the melting process, electrical energy is converted to thermal energy by means of an electrical arc created between the melted metal and the electrodes. An electric arc is characterized by a high current and low voltage. The EAF conditions vary significantly during the four operating processes: charging, boring, melting, and refining. The arc length increases from the boring phase, where the metals start to melt, to the refining phase, where the metals are completely melted, and gradually becomes constant [8]. Charging is the

first phase in which solid scrap metal is loaded into the furnace. An electric arc is then created in the middle of the scrap metal stack. The current exhibits a rather stochastic behavior and a very high deterioration in power quality occurs. When a hole is formed in the middle of the scrap metal stack, the arc becomes more stable (in the melting phase), and 15% of the scrap metal in the solid state becomes liquid. The current remains unstable because the scrap metal is still in a solid state and is not fully melted. In the refining phase, which is the final and most stable arc current behavior observed, the scrap metal is completely melted so that the arc length and demanded current do not vary significantly [9].

There are many publications in the literature related to EAF modeling [10-29]. Different methods are used to describe the electrical arc in these studies. In [10,11], balanced steady-state equations, which are highly beneficial in computational work, are presented. However, only the balanced state of three-phase currents is considered in these equations [12]. A few models presented in the literature have been adapted from the stochastic characteristics of the EAF, which are suitable for voltage flicker analysis [13,14]. In [15,16], differential equations based on time-domain methods are brought forward. In time-domain analysis, the parameters are specified according to the harmonic source voltages and unbalanced three-phase currents. One of the preferred methods for analyzing the arc model in the time domain is based on the Cassie-Mayr equations [16]. Cassie and Mayr's equations are utilized for the low voltage and high currents of the arc, respectively. In [17], different Cassie–Mayr model variants have been investigated and two generalized types of the original Cassie–Mayr model are developed using a large number of recorded actual data. In [18], the characteristics of the arc is evaluated using the physical principles of Mayr with a new EAF model developed using the Monte Carlo method in ATP/EMTP simulation environment. In [19], a dynamic model of an EAF is presented for the estimation of voltage flicker in a power transmission network. The model is based on simulating the varying resistance of an electric arc in the time domain. The frequency-domain characteristics of the EAF is analyzed in [20]. In [21], a linearization and approximation method is proposed and the performance of the EAF has been analyzed. In this method, the arc voltage can be deduced adaptively depending on the arc current by examining the V-I characteristic of the arc furnace. Esfahani and Vahidi [22] carried out a study using the actual values of EAFs of the Mobarakeh Steel Company and come up with a new stochastic model of EAF based on Hidden Markov theory. The effects of flicker have been investigated through a designed IEC flicker meter. In [23], a mathematical model has been constructed using the experimentally obtained average dynamic Volt-Ampere characteristics. In [24], another mathematical EAF model based on field data is developed using an ellipse equation. In [25], a detailed model of the EAF has been built up by using a multibody dynamics (MBD) environment with the finite-element method (FEM). The effects of the arc dynamics and magnetic induction among the phases have been analyzed through a multiphysics approach. In recent years, the number of studies [26-28] on EAF modeling by taking advantage of artificial neural networks (ANN) and field data has increased. In [26], a data-driven neural-network-based nonlinear model has been put forward for the EAF v-i characterization of the time and frequency domains. In [27], an EAF model has been addressed by considering the time-varying arc length as the input parameter of the ANN to generate the voltage and current waveforms of the EAF. In [28], a hybrid discrete wavelet transform (DWT) and radial basis function neural network (RBFNN)-based approach has been introduced to model the dynamic voltage-current characteristics of the EAF. In [29], new models based on long short-term memory (LSTM) networks that are compatible with different operating conditions of the EAF have been developed. In [30], two improved EAF models based on the Schavemaker model, in which the time-varying behaviors of the model parameters are characterized by ARMA models, have been derived. Two recently published papers [31,32] focusing on the optimization of EAF parameters are brought to the attention. In [31], a multi-objective optimization technique has been recommended for the estimation of the EAF parameters under different conditions in a steel plant in Saudi Arabia. In [32], several optimization

algorithms have been combined and used to increase the efficiency of the EAF and reduce energy consumption by minimizing controllable losses. In [33], the parameters and characteristics of several time-domain methods, such as piecewise linear, modified piecewise linear, hyperbolic, and exponential, have been optimized using genetic algorithm and particle swarm optimization for EAF modeling and simulation.

This paper presents a dynamic model of the EAF based on nonlinear time-variant resistance in the time domain for voltage flicker analysis in electrical power systems. In the dynamic model of the EAF, the arc length can be adjusted to simulate the current and voltage waveforms under different EAF operating conditions. A flicker meter in compliance with the International Electrotechnical Commission (IEC) standard has been designed to measure the short-term flicker severity index caused by the EAF in the power system. The suggested dynamic model of the EAF is verified through simulation studies by comparing it with the field data-based model.

The remainder of this paper is organized as follows. Section 2 presents the design and modeling of the EAF. In Section 3, the model of a digital flickermeter designed in PDCAD/EMTDC environment based on IEC standard 61000-4-15 is described. The simulation results are discussed in Section 4. Finally, Section 5 provides the conclusions and significant contributions of this study.

2. DESIGN AND MODELING OF THE EAF

To simulate the stochastic behavior of the EAF, it is necessary to have a dynamic and robust mathematical model that can adapt to different operating conditions such as charging, drilling, melting, and refining. In this study, a mathematical model based on the Cassie arc equation equipped with arc-length modulation has been developed. The EAF can be modeled by a variable arc resistance R_{arc} for each phase, and can be described dynamically by the following differential equations [34]:

$$\frac{dR_{arc}}{dt} = \frac{R_{arc}}{\vartheta_c}\left(1 - \frac{V_{eaf}^2}{V_{arc}^2}\right) \tag{1}$$

$$R_{arc} = \frac{1}{\vartheta_c}\int R_{arc}\left(1 - \frac{\left(R_{arc} i_{arc}\right)^2}{V_{arc}^2}\right) dt \tag{2}$$

where ϑ_c is represented as the de-ionizing time constant (also called relative rate of conductance decrease), V_{eaf} is defined as the instantaneous value of the arc voltage, and V_{arc} indicates the asymptotic arc voltage reached when the arc current (i_{arc}) goes to infinity as given in Eq. (3).

$$V_{arc} = \lim_{i_{arc}\to\infty}\left(V_{eaf}\right) \tag{3}$$

The arc length varies according to the power system of the EAF to be modeled and is inversely proportional to the arc current. Arc length consists of two parts as the constant arc length and the arc length modulation. The constant arc length is adjusted to acquire the operating region at the rated power of the EAF. The arc length modulation is then applied to model the fluctuations in currents occurred by the EAF and is the part representing the "flicker" actually. In Eq. (4), V_{arc} is expressed independently of the arc current [35]:

$$V_{arc} = A + Bl_o + B\Delta l(t) = A + B\left(l_o + \Delta l(t)\right) \tag{4}$$

where A is a constant denoting the voltage drop in the anode and cathode electrodes of the EAF, B is the voltage drop per unit length across the arc, and l_o is the arc length. The arc-length modulation is realized by controlling $\Delta l(t)$, as described in Eq (5).

$$\Delta l(t) = D\sin 2\pi f_m t \tag{5}$$

where D is the parameter that adjusts the flicker level, and f_m is the modulation frequency.

In this study, sinusoidal modulation has been preferred, in which a single modulation frequency (f_m) is used to represent all fluctuations within the worst case. Sinusoidal modulation can be implemented by using a modulation frequency

changing with time. To simulate a practical EAF adequately, the characteristic arc-length fluctuations have to be determined by taking field measurements. Another way of controlling the desired flicker level is to create random flicker modulation with a band-pass-filtered white noise signal. To band-limit the noise, a fourth-order-band-pass filter with the cut-off frequencies of 4 and 14 Hz is used. The amplitude of the noise could then be tuned to obtain the desired flicker level.

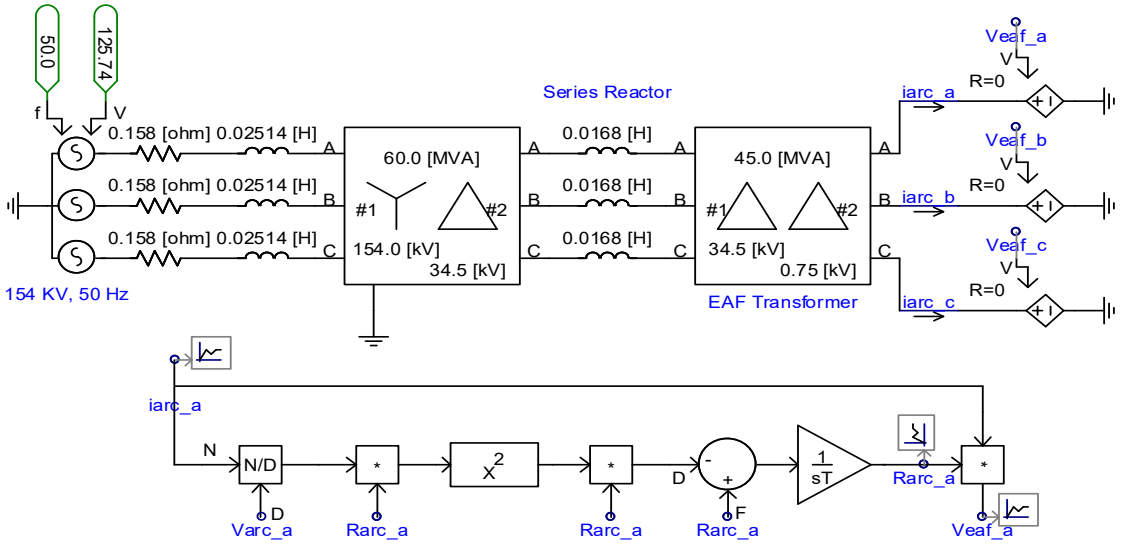

Figure 2. Simulation model of the arc equation and arc length modulation

The simulation model of the arc equation and arc-length modulation implemented for a single phase is demonstrated in Figure 2. The EAF is modeled as a controlled voltage source (V_{eaf}). The arc voltage (V_{arc}) is obtained using Eq. (4) and is utilized in the calculation of arc resistance (R_{arc}). The EAF voltage is found by multiplying the measured arc current (i_{arc}) with the calculated arc resistance (R_{arc}). The initial value of R_{arc} is defined as 0.001 ohm, and the integral time constant is 0.0003 s. The solution time step is specified as 20 µs in PSCAD/EMTDC.

The simulation parameters of the power system and EAF are provided in Table 1. In the developed model, the EAF has a rated power of 40 MW and is connected to the PCC at a 34.5 kV voltage level with a 0.75/34.5 kV distribution transformer and a serial reactor. It is connected to the transmission line with a 154/34.5 kV step-down transformer.

The transmission line impedance is calculated in accordance with the actual system values, and the parameters of the transformer are determined by taking the transformer label values used in field applications as a reference.

Table 1. Simulation parameters

Parameter	Value
Utility Grid (HV source)	154 kV, 50 Hz
Grid Impedance (Z_s)	0.158 Ω + 25.14 µH
HV/MV Power Transformer	154/34.5 kV, 60 MVA, %Uk= 14%
MV/LV EAF Transformer	34.5/0.75 kV, 45 MVA, %Uk= 9%
Serial Reactor	16.8 µH
Three Phase EAF	24 MVAr, pf = 0.85 Arc length (l_0)= 33.7 cm Frequency modulation (f_m)= 8.8 Hz A=40 V, B=10 V/cm, D=5

3. IEC FLICKERMETER

A flickermeter is an apparatus that can detect any fluctuation in the input voltage signal and calculate an output (short-term and long-term flicker severity

indices) representative of human visual sensation. The flickermeter simulates the dynamic and nonlinear characteristics of the lamp-eye-brain response to define the level of flicker that causes irritation to the human eye. This paper presents a digital flickermeter designed in PSCAD/EMTDC based on IEC standard 61000-4-15 [36], which is widely used to assess flicker severity in practical applications. The flickermeter consists of five series-connected functional blocks, as shown in Figure 3.

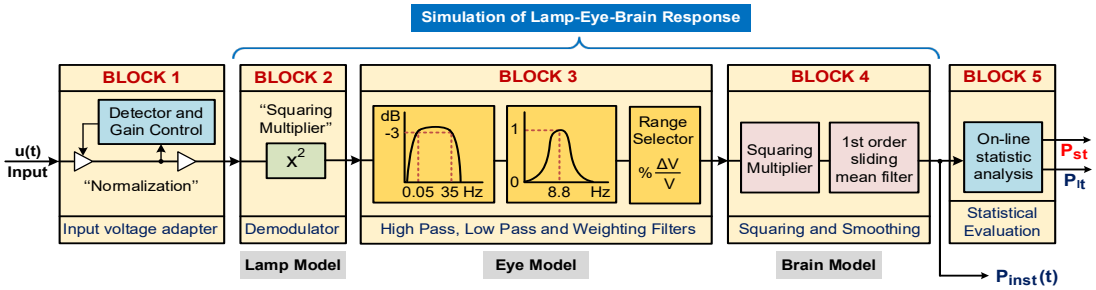

Figure 3. Block diagram of flickermeter model based on the IEC 61000-4-15 [36]

Block 1 is a voltage adapter scales the input voltage level down to an internal reference without changing the voltage fluctuation. The output of block 1 is the normalized signal obtained by dividing the input voltage by its effective value (RMS) at the grid frequency (50 Hz). Block 1 provides a flicker measurement independent of the actual input carrier voltage level.

Block 2, which contains a squaring demodulator to remove the voltage fluctuation from the normalized input signal at the grid frequency, is used to simulate the behavior of an incandescent lamp. The output of block 2 consists of a dc offset, flicker-causing component, and some higher-frequency signals [37].

Block 3 is composed of two filter (band-pass and weighting) circuits in series with each other and simulates the behavior of the human eye. The band-pass filter incorporates first-order high-pass and low-pass filter sections. The 1st order high pass filter (3 dB, 0.05 Hz cutoff frequency as identified in the standard) is used to eliminate the DC offset of the demodulator (block 2) output. The transfer function of the high-pass filter is given in Eq. (6). Subsequently, a low-pass filter (6th order Butterworth filter with a 3 dB cutoff frequency of 35 Hz for 230 V, 50 Hz systems) is applied to remove the double mains frequency ripple components caused by the squaring demodulator block. The transfer function of the low-pass filter is expressed as Eq. (7) and the coefficients used in the equation are provided in Table 2. The weighting filter models the behavior of the lamp–eye system. It is a band-pass filter at the resonant frequency of 8.8 Hz with a gain of 1 [38]. It simulates the frequency response to sinusoidal voltage fluctuations of a coiled filament gas-filled lamp (60 W-230V) combined with the human visual system. The transfer function of the weighting filter is defined in Eq. (8) and the coefficients used in the equation are presented in Table 2 with respect to the IEC standard [36]. The range selector specifies the susceptibility of the flickermeter by modifying the gain as a function of the amplitude of the voltage fluctuation to be measured [39].

$$G_{high}(s) = \frac{s}{s + 2\pi 0.05} \tag{6}$$

$$G_{low}(s) = \frac{1}{1 + b_1\left(\frac{s}{w_c}\right) + b_2\left(\frac{s}{w_c}\right)^2 + b_3\left(\frac{s}{w_c}\right)^3 + b_4\left(\frac{s}{w_c}\right)^4 + b_5\left(\frac{s}{w_c}\right)^5 + b_6\left(\frac{s}{w_c}\right)^6} \tag{7}$$

$$G_{weighting}(s)=\frac{kw_1 s}{s^2+2\lambda s+{w_1}^2}\frac{\left(1+\frac{s}{w_2}\right)}{\left(1+\frac{s}{w_3}\right)\left(1+\frac{s}{w_4}\right)} \quad (8)$$

Table 2. The low pass and weighting filter parameters

Coefficient	Value	Coefficient	Value
b_1	3.864	k	1.74802
b_2	7.464	λ	2π (4.05981)
b_3	9.141	w_1	2π (9.15494)
b_4	7.464	w_2	2π (2.27979)
b_5	3.864	w_3	2π (1.22535)
b_6	1.000	w_4	2π (21.9)

The fourth block includes a squaring multiplier to simulate the nonlinear perception of the flicker and a first-order sliding mean filter to simulate the memory effect in the human brain. The first-order sliding mean filter is derived using Eq. (9), with a time constant (τ) of 300 ms. The output of Block 4 gives the instantaneous flicker sensation, $P_{inst}(t)$, which is then used in the statistical analysis to estimate the short-term flicker severity (P_{st}) and long-term flicker severity (P_{lt}).

$$G_{sliding}(s)=\frac{1}{1+\tau s} \quad (9)$$

A statistical assessment of the instantaneous flicker has been implemented in Block 5 to come out the short and long-term flicker severity, P_{st} and P_{lt}, respectively. The designed flicker meter has been validated by applying the test procedures described in the IEC standard [36], and the error rates obtained according to the performance test results are below the specified tolerance range. The P_{st} is evaluated in a 10-minute time duration, while the P_{lt} is calculated for a 2-hour time period. The statistical calculation required to evaluate the 10-minute P_{st} prescribed in the IEC standard (IEC-61000-4-15) is given below [36]:

$$P_{st}=\sqrt{\begin{matrix}0.0314\,P_{0.1}+0.0525\,P_{1s}+0.0657\,P_{3s}\\+0.28\,P_{10s}+0.08\,P_{50s}\end{matrix}} \quad (10)$$

where:

$$\begin{aligned}P_{50s}&=(P_{30}+P_{50}+P_{80})\,/\,3\\P_{10s}&=(P_6+P_8+P_{10}+P_{13}+P_{17})\,/\,5\\P_{3s}&=(P_{2.2}+P_3+P_4)\,/\,3\\P_{1s}&=(P_{0.7}+P_1+P_{1.5})\,/\,3\end{aligned} \quad (11)$$

Here, 0.0314, 0.0525, 0.0657, 0.28 and 0.08 values are the weighting coefficients [40]. P_x is the xth percentile of the P_{inst} values logged during a specified observation time interval, where x is 0.1, 0.7, 1, 1.5, 2.2, 3, 4, 6, 8, 10, 13, 17, 30, 50, and 80, respectively [41].

The following formula can also be used to obtain the long-term flicker severity, P_{lt}, for the last 120 minutes by taking 12 samples of P_{st}:

$$P_{lt}=\sqrt[3]{\frac{1}{N}\sum_{i=1}^{N}P_{st,i}} \quad (12)$$

where P_{lt} is the long-term flicker coefficient, $P_{st,k}$ is the kth consecutive value of the short-term coefficient, and N=12 is the number of P_{st} levels taken to compute the P_{lt} coefficient [41].

4. SIMULATION RESULTS AND DISCUSSION

The EAF has been modeled as a voltage-controlled nonlinear load on the secondary side (0.75 kV) of the EAF transformer. The arc length (l_0) has been chosen as 33.7 cm, the frequency modulation has been determined as 8.8 Hz and the parameters of the arc modulation have been assigned with respect to the values given in Table 1. The voltage and current waveforms of the EAF on the low-voltage side of the EAF transformer are displayed in Figure 4. The variation in the arc resistance over time and the i-v characteristic waveform of the EAF at the secondary side (0.75 kV level) of the transformer during balanced operation are depicted in Figure 5 and 6 respectively.

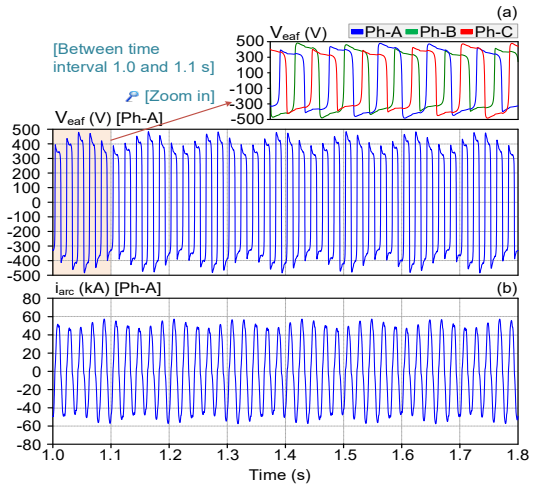

Figure 4. **(a)** EAF voltage (V_{eaf}) waveform at 0.75 kV level of the EAF transformer **(b)** Arc current (i_{arc}) waveform at 0.75 kV level of the EAF transformer

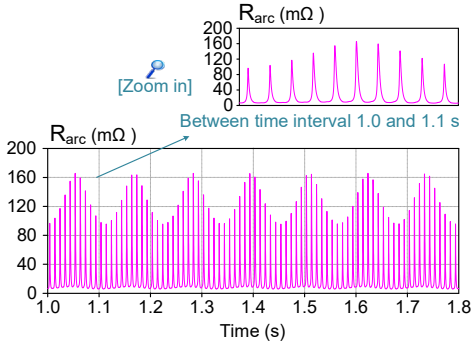

Figure 5. The variation of the arc resistance over time

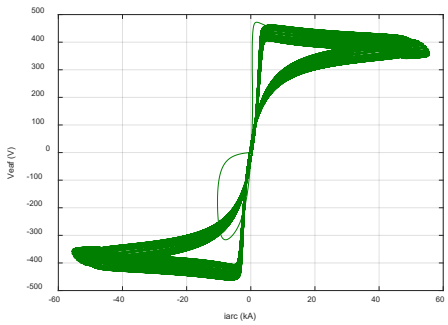

Figure 6. i-v characteristic waveform of the EAF at the secondary side (0.75 kV level) of the transformer

The current and voltage waveforms of the EAF seen from the high-voltage side of the EAF transformer and the i-v characteristic curve obtained at the primary side of the EAF transformer during balanced operation are illustrated in Figure 7 and 8 respectively.

The short-term flicker severity (P_{st}) during stable operation of the EAF is shown in Figure 9. The P_{st} has been obtained as 5.253 when the arc length is 33.7 cm and the flicker level affecting the arc length modulation is 5.

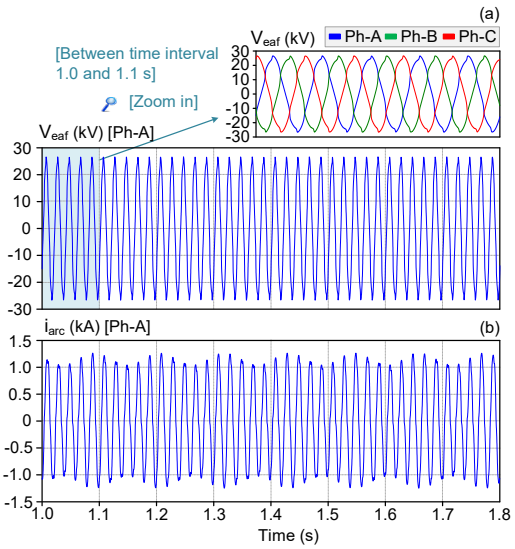

Figure 7. **(a)** EAF Voltage (V_{eaf}) waveform at 34.5 kV level of the EAF transformer **(b)** Arc Current (i_{arc}) waveform at 34.5 kV level of the EAF transformer

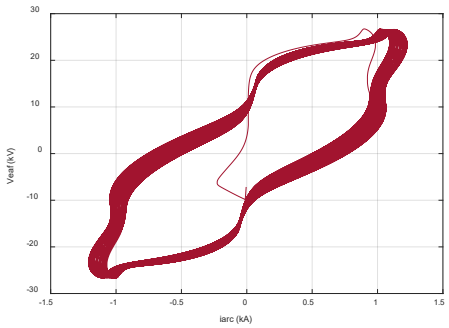

Figure 8. i-v characteristic waveform of the EAF at the primary side (34.5 kV level) of the transformer

The harmonic content of the arc current for phase A and the total harmonic distortion (THD) during stable operation of the EAF are provided in Table 3. It can be inferred that the amplitudes of the 3rd and 5th low-order harmonics are high in the arc current at the primary side of the EAF transformer, and the THD is 10.63%.

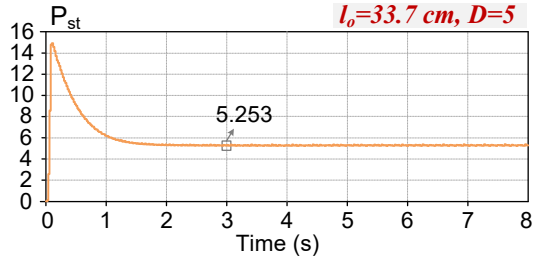

Figure 9. Short-term flicker severity during the stable operation of the EAF

Figure 10 represents the simulation results for the arc length and flicker-level change. When the arc length increases from 33.7 cm to 37.5 cm and the flicker level changes from 3 to 5 at t=3 s, it is clearly seen that the arc current, the active and reactive powers of the EAF decrease while the arc resistance, the arc voltage, and the power factor increase. Figure 11 shows that the short-term flicker severity sets from 3.145 to 6.251 during the arc length and flicker level change.

Table 3. Harmonic content of the arc current (Phase-A)

Harmonic order	Percent (%)	Harmonic order	Percent (%)
Fundamental	100	17	0.104
2	2.233	18	0.367
3	4.834	19	0.309
4	1.241	20	0.365
5	8.534	21	0.228
6	0.514	22	0.389
7	2.074	23	0.302
8	0.465	24	0.393
9	0.908	25	0.273
10	0.645	26	0.387
11	0.976	27	0.416
12	0.373	28	0.490
13	0.428	29	0.508
14	0.406	30	0.626
15	0.279	31	0.667
16	0.460	**THD**	**10.63**

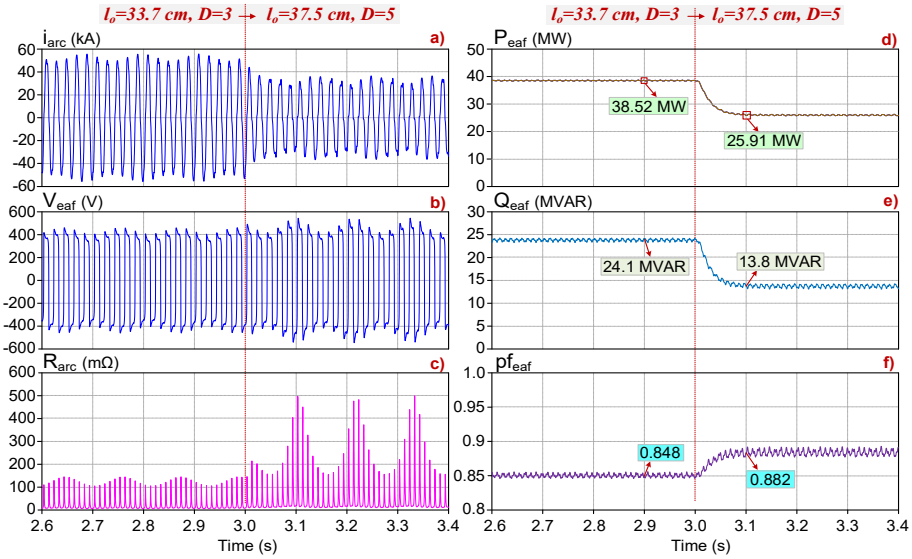

Figure 10. Simulation results during the arc length and flicker level change **(a)** Arc current (i_{arc}) waveform at 0.75 kV level of the EAF transformer for phase-A **(b)** EAF voltage (V_{eaf}) waveform at 0.75 kV level of the EAF transformer for phase-A **(c)** The arc resistance (R_{arc}) for phase-A **(d)** The active power of the EAF **(e)** The reactive power of the EAF **(f)** The power factor of the system

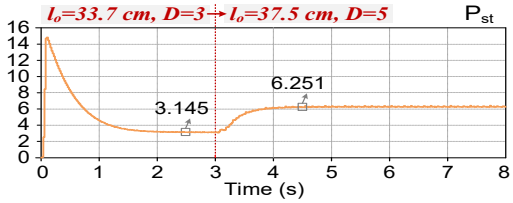

Figure 11. Short-term flicker severity during the arc length and flicker level change

5. COMPARISON WITH ACTUAL OPERATION DATA

To show the effectiveness of the dynamic model of the EAF, another model based on actual operation data is developed in PSCAD/EMTDC, as presented in Figure 12. Field data is collected from an iron and steel factory located in Iskenderun, Turkey, with a sampling rate of 3.6 kS/s. It consists of variable resistance and inductance, which are computed using the measured values of the instantaneous line-to-neutral voltage and line current of the EAF on the MV side. Hence, the real dynamic behavior of the EAF is represented by a variable resistor and an inductor in each phase. The field data is recorded within one minute duration when the EAF is in the refining operation mode. Figure 13 shows the variation in the arc resistance and inductance for each phase over time.

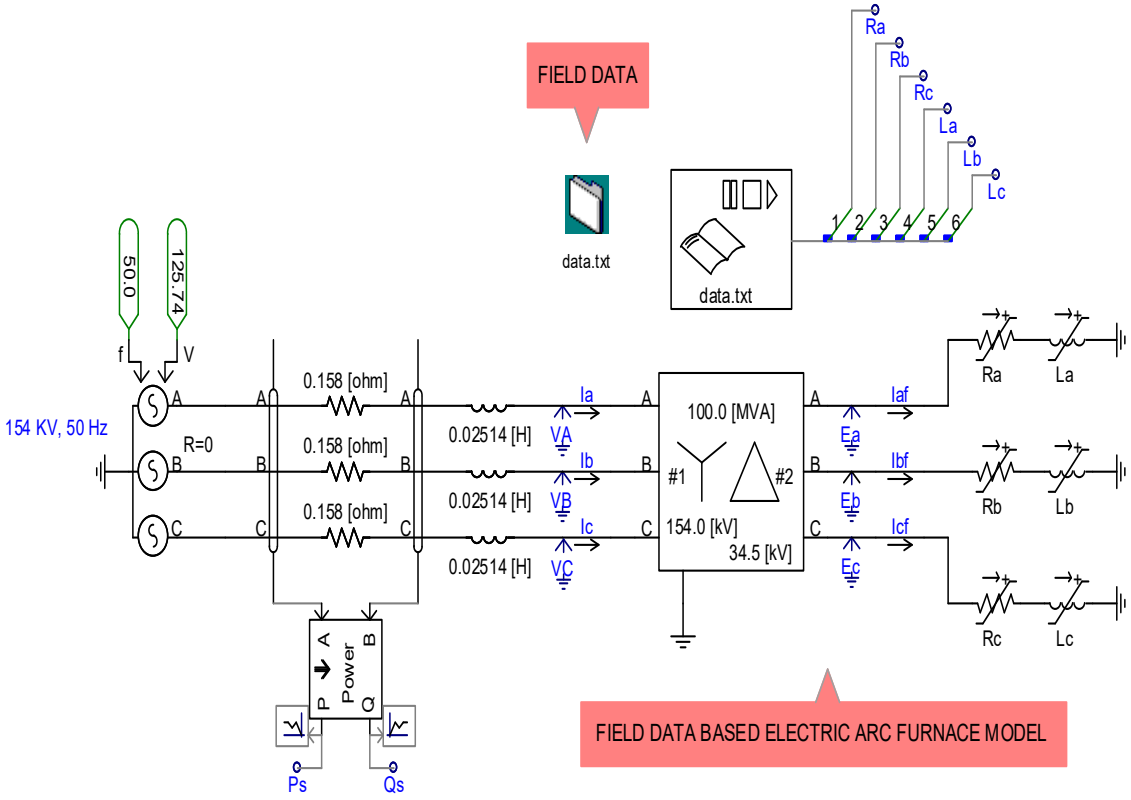

Figure 12. Simulation model of the EAF based on the field data

As in the dynamic model of the EAF, the network is designed to be 154 kV, 50 Hz and the short-circuit power is taken as 3000 MVA. The step-down transformer is modeled as having a conversion ratio of 154/34.5 kV, a rated power of 100 MVA, and a %Uk (the transformer short-circuit impedance voltage) of 12%. time.

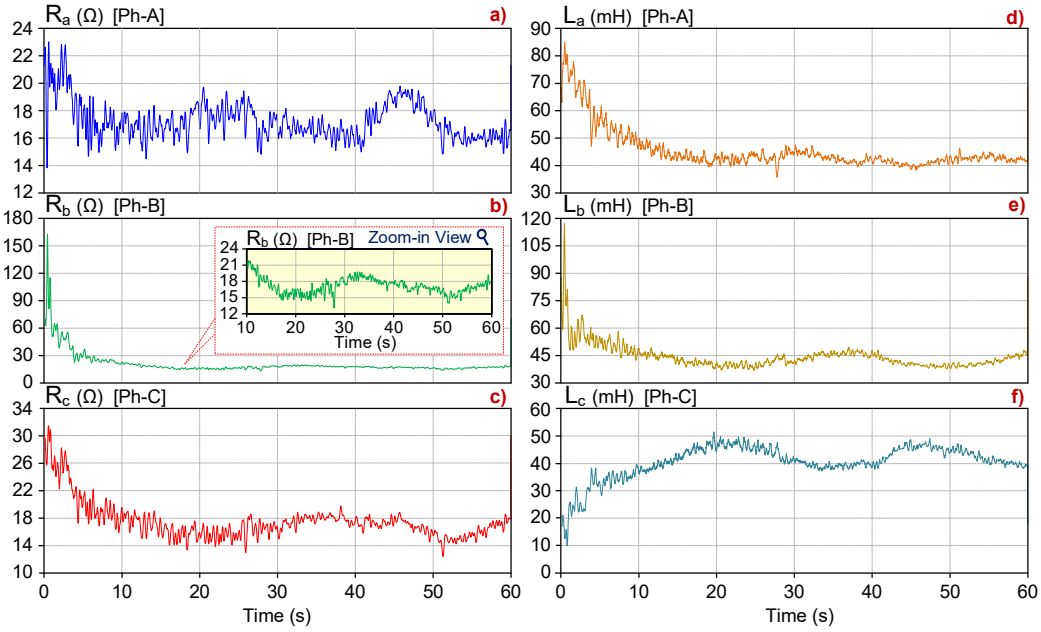

Figure 13. Arc resistance and inductance values for each phase

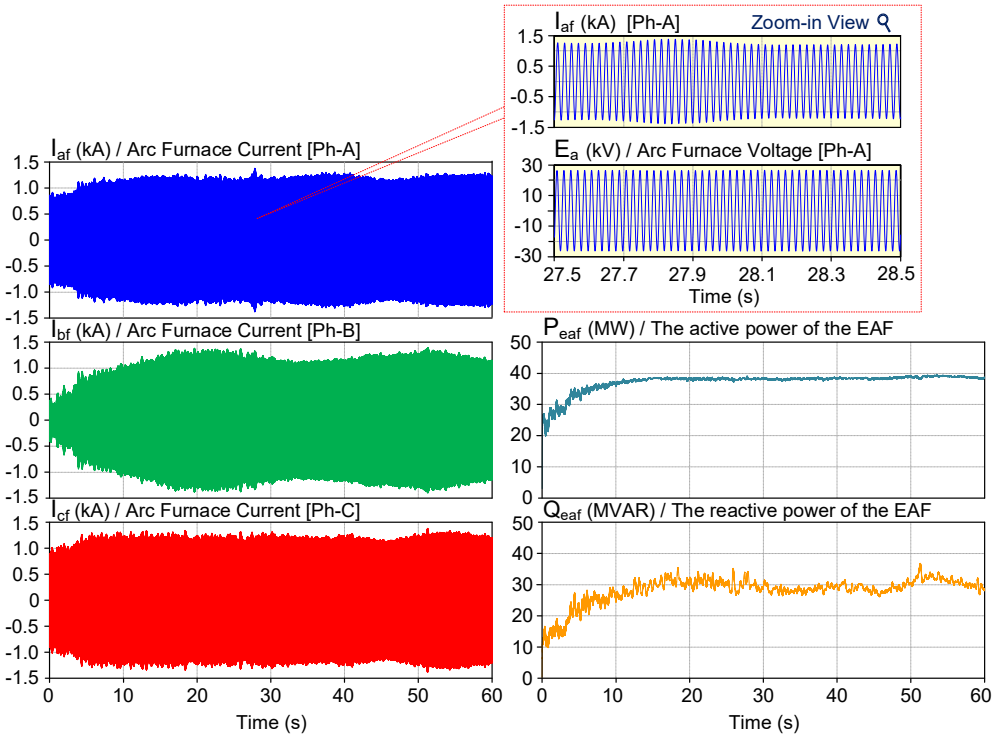

Figure 14. Current, active power and reactive power waveforms of the EAF

The three-phase currents drawn by the EAF (I_{af}, I_{bf}, and I_{cf}), active power of the EAF (P_{eaf}), and reactive power of the EAF (Q_{eaf}) are shown in Figure 14. When the current waveforms are examined, it is clear that a random flicker occurs instead of a sinusoidal flicker, unlike the dynamic arc furnace model. However, it is understood that the i-v characteristic of the EAF obtained from the model based on the field data, which is presented in Figure 15, is similar to that of the developed dynamic model.

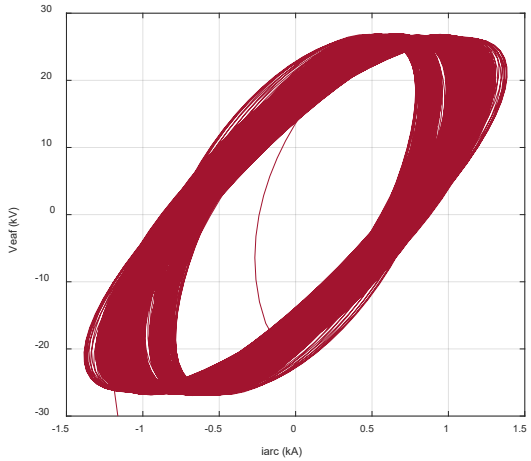

Figure 15. i-v characteristic waveform of the EAF with field data

6. CONCLUSION

An accurate and dynamic mathematical model of the EAF, whose parameters can be adjusted according to different operating conditions, is needed to analyze the voltage flicker problem and offer solution alternatives. In this study, a dynamic EAF load model in the time domain has been developed by considering the rapidly changing, unstable, and nonlinear behavior of the electrical arc over time. The EAF model has been verified through simulation studies performed in PSCAD/EMTDC environment. Moreover, the simulation results of the dynamic model of the EAF have been compared with the results obtained from the model based on the field data collected from an iron and steel factory located in Iskenderun. The current-voltage characteristic of the dynamic EAF model clearly shows the stochastic change of the arc length. The arc caused by the EAF load at the busbar voltage was evaluated by measuring the short-term flicker intensity index using a flicker meter designed in accordance with the IEC 61000-4-15 standard. It has been shown that the developed EAF model and designed flicker meter can be used to identify and analyze voltage flicker problems. It is envisaged that the developed EAF model will constitute a preliminary step for practical applications and assist in evaluating solutions that will alleviate the effect of EAFs on power systems.

Further research will focus on modeling the ladle furnace (LF) load and analyzing different power quality problems such as harmonics, interharmonics, and current/voltage imbalances caused by EAF and LF loads in the power system. In addition, studies will be carried out on C-type harmonic filter designs and modeling of custom power devices such as Static Var Compensator or Static Synchronous Compensator to solve these problems.

7. REFERENCES

1. Alves, M.F., Peixoto, Z.M.A., Garcia, C.P., Gomes, D.G., 2010. An Integrated Model for the Study of Flicker Compensation in Electrical Networks. Electric Power Systems Research, 80(10), 1299-1305.

2. Balouji, E., Bäckström, K., McKelvey, T., Salor, Ö., 2020. Deep-Learning-Based Harmonics and Interharmonics Predetection Designed for Compensating Significantly Time-Varying EAF Currents. IEEE Transactions on Industry Applications, 56(3), 3250-3260.

3. Göl, M., Salor, Ö., Alboyacı, B., Mutluer, B., Çadırcı, I., Ermis, M., 2010. A New Field-Data-Based EAF Model for Power Quality Studies. IEEE Transactions on Industry Applications, 46(3), 1230-1242.

4. Thales, A.C.M., Virna, C.O., 2022. Survey on the Electric Arc Furnace and Ladle Furnace Electric System. Ironmaking & Steelmaking, 49(10), 976-994.

5. Altıntaş, E., Salor, Ö., Çadırcı, I., Ermis, M., 2010. A New Flicker Contribution Tracing

Method Based on Individual Reactive Current Components of Multiple EAFs at PCC. IEEE Transactions on Industry Applications, 46(5), 1746-1754.

6. Logoglu, E.U., Salor, O., Ermis, M., 2019. Real-Time Detection of Interharmonics and Harmonics of AC Electric Arc Furnaces on GPU Framework. IEEE Transactions on Industry Applications, 55(6), 6613-6623.

7. Hay, T., Visuri, V.-V., Aula, M., Echterhof, T., 2021. A Review of Mathematical Process Models for the Electric Arc Furnace Process. Steel Research International, 92(3), 2000395.

8. Seker, M., Memmedov, A., Huseyinov, R. Kockanat, S., 2017. Power Quality Measurement and Analysis in Electric Arc Furnace for Turkish Electricity Transmission System. Elektronika Ir Elektrotechnika, 23(6), 25-33.

9. Göl, M., 2009. A New Field-Data Based EAF Model Applied to Power Quality Studies. M.Sc. Thesis, Middle East Technical University, Institute of Natural and Applied Sciences, Department of Electrical and Electronics Engineering, Ankara, 88.

10. Mayordomo, J.G., Beites, L.F., Asensi, R. Izzeddine, M., Zabala, L., Amantegui, J., 1997. A New Frequency Domain Arc Furnace Model for Iterative Harmonic Analysis. IEEE Transactions on Power Delivery, 12(4), 1771-1778.

11. Beites, L.F, Mayordomo, J.G., Hernandes, A., Asensi, R., 2001. Harmonics, Inter Harmonic, Unbalances of Arc Furnaces: A New Frequency Domain Approach. IEEE Transactions on Power Delivery, 16(4), 661-668.

12. Hooshmand, R., Banejad, M., Esfahani, M.T., 2008. A New Time Domain Model for Electric Arc Furnace. Journal of Electrical Engineering, 59(4), 195-202.

13. Wang, F., Jin, Z., Zhu, Z., Wang, X., 2005. Application of Extended Kalman Filter to the Modelling of Electric Arc Furnace for Power Quality Issues. International Conference on Neural Networks and Brain, Beijing, 991-996.

14. Pak, L.-F., Dinavahi, V., 2007. Real-Time Digital Time-Varying Harmonic Modelling and Simulation Techniques. IEEE Transactions on Power Delivery, 22(2), 1218-1227.

15. Bellido, R.C., Gomez, T., 1997. Identifcation and Modelling of a Three Phase Arc Furnace for Voltage Disturbance Simulation. IEEE Transactions on Power Delivery, 12(4), 1812-1817.

16. Mokhtari, H., Hejri, M., 2002. A New Three Phase Time-Domain Model for Electric Arc Furnaces Using MATLAB. IEEE/PES Transmission and Distribution Conference and Exhibition, Yokohama, 2078-2083.

17. Golestani, S., Samet, H., 2016. Generalised Cassie–Mayr Electric Arc Furnace Models. IET Generation, Transmission & Distribution, 10(13), 3364-3373.

18. Plata, E.A.C., Farfan, A.J.U., Marin, O.J.S., 2015. Electric Arc Furnace Model in Distribution Systems. IEEE Transactions on Industry Applications, 51(5), 4313-4320.

19. Teklic, A.T., Filipovic-Grcic, B., Pavic, I., 2017. Modelling of Three-Phase Electric Arc Furnace for Estimation of Voltage Flicker in Power Transmission Network. Electric Power Systems Research, 146, 218-227.

20. Ting, W., Wennam, S. Yao, Z., 1997. A New Frequency Domain for the Harmonic Analysis of Power System with Arc Furnace. Fourth International Conference on Advances in Power System Control, Operation and Management, (APSCOM), Hong Kong, 552-555.

21. Zheng, T., Makram, E.B., 2000. An Adaptive Arc Furnace Model. IEEE Transactions on Power Delivery, 15(3), 931-939.

22. Esfahani, M.T., Vahidi, B., 2012. New Stochastic Model of Electric Arc Furnace Based on Hidden Markov Model: A Study of Its Effects on the Power System. IEEE Transactions on Power Delivery, 27(4), 1893-1901.

23. Lozynskyy, A., Kozyra, J., Łukasik, Z., Kuśmińska-Fijałkowska, A., Kutsyk, A., Paranchuk, Y., Kasha, L., 2022. A Mathematical Model of Electrical Arc Furnaces for Analysis of Electrical Mode Parameters and Synthesis of Controlling Influences. Energies, 15(5), 1623, 1-19.

24. Lee, C., Kim, H., Lee, E.-J., Baek, S.-T., Shim, J.W., 2021. Measurement-Based Electric Arc Furnace Model Using Ellipse Formula. IEEE Access, 9, 155609-155621.

25. Brusa, E.G.M., Morsut, S., 2015. Design and Structural Optimization of the Electric Arc Furnace Through a Mechatronic-Integrated Modeling Activity. IEEE/ASME Transactions on Mechatronics, 20(3), 1099-1107.

26. Chen, C-I., Chen, Y-C., 2015. A Neural-Network-Based Data-Driven Nonlinear Model on Time- and Frequency-Domain Voltage–Current Characterization for Power-Quality Study. IEEE Transactions on Power Delivery, 30(3), 1577-1584.

27. Segura, R.G., Castillo, J.V., Chavez, F.M., Gandara, O.L., Aguilar, J.O., 2017. Electric Arc Furnace Modeling with Artificial Neural Networks and Arc Length with Variable Voltage Gradient. Energies, 10, 1424, 1-11.

28. Chang, G.W., Shih, M-F., Chen, Y-Y., Liang, Y-J., 2014. A Hybrid Wavelet Transform and Neural Network-Based Approach for Modelling Dynamic Voltage-Current Characteristics of Electric Arc Furnace. IEEE Transactions on Power Delivery, 29(2), 815-824.

29. Klimas, M., Grabowski, D., 2023. Application of Long Short-Term Memory Neural Networks for Electric Arc Furnace Modeling. Applied Soft Computing, 145, 110574.

30. Babaei, Z., Samet, H., Jalil, M., 2023. An Innovative Approach Considering Active Power and Harmonics for Modeling the Electric Arc Furnace Along With Analyzing Time-Varying Coefficients Based on ARMA Models. International Journal of Electrical Power and Energy Systems, 153, 109377.

31. Illahi, F., El-Amin, I., Mukhtiar, M.U., 2018. The Application of Multiobjective Optimization Technique to the Estimation of Electric Arc Furnace Parameters. IEEE Transactions on Power Delivery, 33(4), 1727-1734.

32. Saboohi, Y., Fathi, A., Skrjanc, I., Logar, V., 2019. Optimization of the Electric Arc Furnace Process. IEEE Transactions on Industrial Electronics, 66(10), 8030-8039.

33. Nooshabadi, A.M.E., Sadeghi, S., Hashemi-Dezaki, H., 2022. Optimal Electric Arc Furnace Model's Characteristics Using Genetic Algorithm and Particle Swarm Optimization and Comparison of Various Optimal Characteristics in DIgSILENT and EMTP-RV. International Transactions on Electrical Energy Systems, 9952315, 1-20.

34. Cassie, A.M., 1939. A New Theory of Rupture and Circuit Severity. CIGRÉ Technical Report 102, Paris, 14.

35. Larsson, T., 1998. Voltage Source Converters for Mitigation of Flicker Caused by Arc Furnaces. Ph.D. Thesis, KTH, Superseded Departments, Electric Power Systems, 203.

36. IEC Standard 61000-4-15:2010. Electromagnetic Compatibility (EMC) - Part 4-15: Testing and Measurement Techniques - Flickermeter - Functional and Design Specifications, 83.

37. Hooshyar, A., El-Saadany, E.F., 2013. Development of a Flickermeter to Measure Non-Incandescent Lamps Flicker. IEEE Transactions on Power Delivery, 28(4), 2103-2115.

38. Wiczynski, G., 2012. Inaccuracy of Short-Term Light Flicker Pst Indicator Measuring with a Flickermeter. IEEE Transactions on Power Delivery, 27(2), 842-848.

39. Bertola, A., Lazaroiu, G.C., Roscia, M., Zaninelli, D., 2004. A Matlab-Simulink Flickermeter Model for Power Quality Studies. 11th International Conference on Harmonics and Quality of Power, IEEE, Lake Placid, NY, USA, 734-738.

40. Onal, Y., Gerek, O.N., Ece, D.G., 2016. Empirical Mode Decomposition Application for Short-Term Flicker Severity. Turkish Journal of Electrical Engineering & Computer Sciences, 24, 499-509.

41. Kołek, K., Firlit, A., Piatek, K., Chmielowiec, K., 2021. Analysis of the Practical Implementation of Flicker Measurement Coprocessor for AMI Meters. Energies, 14, 1589.